High density fluorocarbon etching of silicon in an inductively coupled plasma: Mechanism of etching through a thick steady state fluorocarbon layer

T. E. F. M. Standaert,[a] M. Schaepkens, N. R. Rueger, P. G. M. Sebel,[b] and G. S. Oehrlein[c]
Department of Physics, State University of New York at Albany, Albany, New York 12222

J. M. Cook
Lam Research Corporation, Fremont, California 94538-6470

(Received 5 May 1997; accepted 15 September 1997)

For various fluorocarbon processing chemistries in an inductively coupled plasma reactor, we have observed relatively thick (2–7 nm) fluorocarbon layers that exist on the surface during steady state etching of silicon. In steady state, the etch rate and the surface modifications of silicon do not change as a function of time. The surface modifications were characterized by *in situ* ellipsometry and x-ray photoelectron spectroscopy. The contribution of direct ion impact on the silicon substrate to the etching mechanism is reduced with increasing fluorocarbon layer thickness. Therefore, we consider that the silicon etch rate is controlled by a neutral etchant flux through the layer. Our experimental data show, however, that ions play an import role in the transport of silicon etching precursors through the layer. A model is developed that describes the etch kinetics through a fluorocarbon layer based on a fluorine diffusion transport mechanism. The model is consistent with the data when one or two of the following roles of the ions on the etching process are assumed. The first role is an enhancement in the diffusivity of fluorine atoms through the fluorocarbon layer and an enhancement in the reaction probability of fluorine in the fluorocarbon layer. In this case the fluorine is assumed to originate from the gas phase. The second role includes ion fragmentation and dissociation of the fluorocarbon surface molecules. © *1998 American Vacuum Society.*
[S0734-2101(98)02201-5]

I. INTRODUCTION

High density plasma (HDP) SiO_2 etching processes are currently being developed to replace the conventional SiO_2 etching processes performed using low density reactive ion etching (RIE) tools. High ion densities and relatively low operating pressures ($\sim 1-10$ mTorr) allow highly anisotropic and fast etching, which are important requirements in future semiconductor manufacturing. The planar coil inductively coupled plasma (ICP) reactor[1] is a promising candidate for meeting these and other demands, such as high process uniformity over large area wafers.

For contact hole etching through insulating films, high selectivity with respect to the underlying material is required. Recently, Rueger *et al.*[2] reported data from an initial study of selective etching of SiO_2 over Si in the ICP reactor, where a selectivity of 40 is achieved using fluorocarbon gases. Highly selective etching of SiO_2 to Si is suggested to be due to the different etching mechanisms of the materials.[2–8] The etching of both materials occurs through a fluorocarbon film. In the case of SiO_2, this fluorocarbon film is very thin (typically less than 1 nm) and a reactive ion sputtering process is observed.[9] This article will show that silicon etching is regulated by a relatively thick fluorocarbon layer (2–7 nm), which protects the silicon from direct ion impact. Oehrlein *et al.*[10,11] proposed a neutral transport mechanism for RIE etching of silicon through a thick fluorocarbon layer. However, in a HDP environment it will be shown that in addition to a neutral etchant flux ions also play an important role in the Si etching mechanism. A model extended to account for this role of ions will be presented.

II. EXPERIMENTAL SETUP

The ICP or transformer coupled plasma (TCP) reactor that is used in our work is similar to the one described by Keller *et al.*[1] with the exception that magnets were not installed in our multipole bucket. Figure 1 shows a cross sectional view. The vacuum in the chamber is separated from atmosphere by a 19-mm-thick quartz coupling window with a diameter of 23 cm. For the plasma generation, a planar coil with a diameter of 16 cm is placed at the atmospheric pressure side of the window and supplies inductively power (0–1400 W, 13.56 MHz) to the discharge. The rf current through the coil induces a current in the plasma generation region which is confined to a small region (2–3 cm) below the coupling window.[12] The gas is injected into the plasma generation region by a gas feed ring under the coupling window. During the generation, the plasma diffuses over a few mean free paths to a 125 mm wafer which is located 7 cm under the

[a]Electronic mail: standaer@cnsvax.albany.edu
[b]Permanent address: Eindhoven University of Technology, P.O. Box 513, 5600 MB Eindhoven, The Netherlands.
[c]Electronic mail: oehrlein@cnsibm.albany.edu

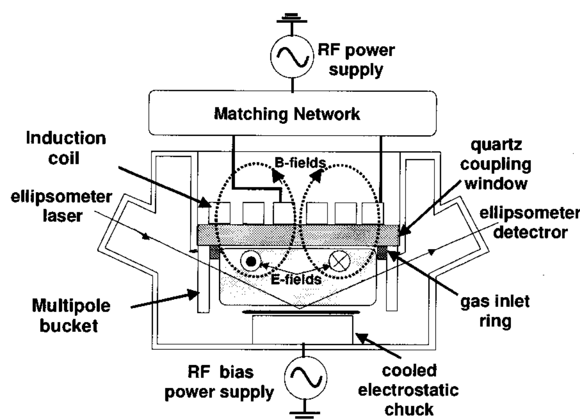

FIG. 1. Schematic of the experimental apparatus.

coupling window. The planar coil design results in a highly uniform ion current density across the wafer (<7% from center to edge).[13]

The wafer is clamped by an electrostatic chuck cooled to 10 °C using a circulated coolant. Due to the inductive coupling, a low plasma potential of 15–20 V (Ref. 14) with respect to the floating walls is obtained. This results in low ion impact energies. The energy of the ions impacting on the wafer can be increased independently of the plasma generation by applying a rf bias (0–250 W, 3.4 MHz) to the chuck. The increase in energy is linear with the rf bias power.[13,15] The self bias voltage that is being developed on the wafer was measured with respect to ground using a probe that was attached to the wafer. The floating potential with respect to ground is equal to $+15$ V and the self-bias voltage was varied down to -150 V. Thermal contact between the wafer and chuck is established by a 5 Torr helium pressure at the backside of the wafer. The partial pressure due to a helium leak in the chamber, if any, was less than 0.1 mTorr. The thermal conductivity of helium is about 1000 times lower than the thermal conductivity of the wafer. Therefore, it can be expected that the wafer temperature increases by 20 °C if the bias power is increased to 250 W. The temperature difference between front- and backside of the wafer is estimated to be about 0.1 °C at this bias power.

The base pressure in the chamber was maintained at 5×10^{-6} mbar by a 450 ℓ/s turbomolecular pump backed by a Roots blower and mechanical pump. During experiments the pressure was set at 6 mTorr by an automatic throttle valve in the exhaust line. The gas chemistries used were 40 sccm CHF_3, 20 sccm C_3F_6, 30 sccm C_2F_6, and 20 sccm C_3F_6 admixed with 12 sccm H_2.

The deposition and etch rates were measured using real time *in situ* He–Ne ellipsometry. The ellipsometer is an automated rotating compensator ellipsometer working in the polarizer-compensator-sample-analyzer (PCSA) configuration.[16] A sampling time of 0.5 s gives an accuracy in Ψ and Δ of about 0.01°. The angle of incidence was set at 71.73°. This setup also allows for real time *in situ* surface analysis on crystalline silicon as is described in Refs. 17–19.

More detailed surface information was obtained using x-ray photoelectron spectroscopy (XPS) on etched crystalline silicon samples. After real time ellipsometry surface analysis, first the inductive power and, within 1 s, the rf bias power, were turned off in order to maintain the surface modifications that are present during the etching process. The samples were transferred under ultrahigh vacuum (UHV) to a Vacuum Generators ESCA Mk II analysis chamber. Photoelectrons were emitted using a nonmonochromatized Mg $K\alpha$ x-ray source (1253.6 eV). Survey spectra and high resolution spectra of C(1s), Si(2p), F(1s), and O(1s) electron emission were obtained under two emission angles, 75° and 0° with respect to the sample normal. The spectra presented in this article were obtained at a 20 eV pass energy.

B-doped, 3–5 Ω cm (100) silicon was used for surface analysis experiments and for obtaining fluorocarbon etch rates. Samples with a multilayer structure (250 nm polycrystalline Si, 100 nm SiO_2 on a crystalline substrate) were etched to determine the silicon etch rate by ellipsometry. Before loading a sample into the ICP reactor, fluorocarbon residues in the chamber were removed by running an oxygen plasma. After this step, an untreated poly- or crystalline silicon sample was loaded without any initial surface cleaning step, because a native oxide layer is removed in less than a few seconds during the etching process. Before acquiring any data the chamber was seasoned for about 90 s by running a fluorocarbon plasma without any rf bias to cover the walls and the wafer with a fluorocarbon film. Then the bias was turned on and the deposited fluorocarbon film on the wafer was etched back. From this point surface information or etch rates were obtained. For determination of the fluorocarbon etch rate, a fluorocarbon film was deposited at this point without applying any bias and was subsequently etched back. In this way reproducible results were obtained. However, for highly polymerizing conditions, e.g., C_3F_6/H_2, small variations (<20% in the etch rates) between different runs can still be observed. This effect is strongly dependent on the chamber condition[20] and has been extensively studied by Schaepkens *et al.*[21]

Finally, it should be mentioned that all data presented in this article are taken under steady state conditions. This means that the etch rate is constant during the etching of the substrate (silicon or fluorocarbon material). The surface modifications are also constant in case of steady state silicon etching. The fluorocarbon layer that exists on the silicon will be referred to as steady state fluorocarbon layer or CF_x layer.

III. RESULTS AND DISCUSSION

A. Etch rates of silicon and fluorocarbon material

High density fluorocarbon plasmas are well known for their polymer deposition on the substrate.[22,23] This deposition has to be suppressed by applying rf bias power to the substrate in order to establish net etching. The etch rate of a thick fluorocarbon film (>50 nm) is plotted in Fig. 2 as a function of the self-bias voltage and for various feedgas chemistries. Negative values of the fluorocarbon etch rate correspond to fluorocarbon deposition rates under biased

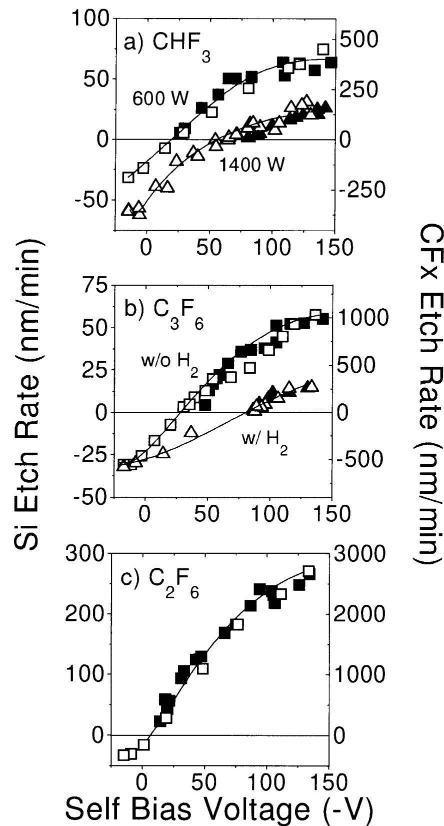

FIG. 2. Silicon (closed symbols) and fluorocarbon (open symbols) etch rates as a function of self-bias voltage for different fluorocarbon plasmas: (a) 40 sccm CHF_3, 6 mTorr, for two inductive powers: squares 600 W, triangles 1400 W; (b) 20 sccm C_3F_6, 6 mTorr, 1400 W, with hydrogen addition: squares 0 sccm H_2; triangles 12 sccm H_2 (c) 40 sccm C_2F_6, 6 mTorr, 1400 W.

conditions. The deposition rates at +15 V were measured without applying any bias (passive deposition). To suppress the fluorocarbon deposition, a minimum self-bias voltage is required. This threshold voltage varies for the different feedgas chemistries and inductive power levels. Beyond this threshold, it is possible to etch silicon, which exhibits a similar etch rate behavior as fluorocarbon material.

Figure 2 suggests that the etching mechanisms of silicon and fluorocarbon material are similar, i.e., the silicon etch rate is proportional to the fluorocarbon etch rate at similar process conditions. This observation is confirmed by the data shown in Fig. 3 where the fluorocarbon etch rate is plotted versus the silicon etch rate. For two pressures, 6 and 20 mTorr, the flow ratio of C_2F_6 and C_3F_6 was increased from 0% to 100% in steps of 20%. The self-bias voltage and inductive power were fixed at −85 V and 1400 W, respectively. By changing the flow ratio or the pressure, both the passive deposition rate and the steady state layer thicknesses on silicon change significantly. However, the ratio of the fluorocarbon etch rate and silicon etch rate remains unaltered.

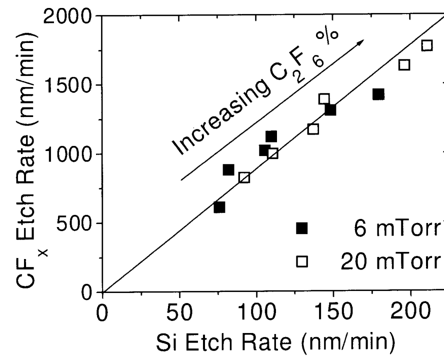

FIG. 3. Fluorocarbon etch rate vs silicon etch rate for two different operating pressures. The flow ratio of C_2F_6 and C_3F_6 was changed in steps of 20% while the self-bias voltage, pressure, and the inductive power were fixed at −85 V, 6 mTorr, and 1400 W, respectively.

B. Surface analysis: Ellipsometry

During the etching process, silicon is exposed to fluorocarbon ions and neutrals. This leads to the fluorination of, and the fluorocarbon film formation on, the silicon surface.[7,19,24,25] In addition to XPS surface analysis, which will be discussed in Sec. III C, real time *in situ* ellipsometry

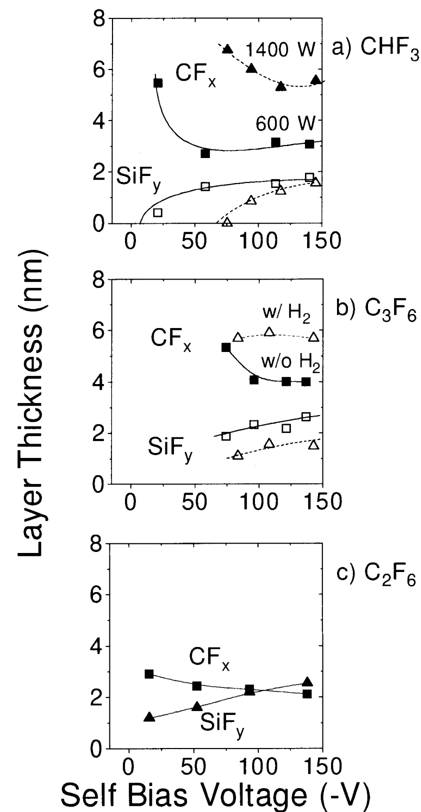

FIG. 4. Steady state CF_x (closed symbols) and SiF_y (open symbols) layer thicknesses as a function of the self-bias voltage for different fluorocarbon plasmas: (a) 40 sccm CHF_3, 6 mTorr, for two inductive powers: squares 600 W, triangles 1400 W; (b) 20 sccm C_3F_6, 6 mTorr, 1400 W, with hydrogen addition: squares 0 sccm H_2, triangles 12 sccm H_2; (c) 40 sccm C_2F_6, 6 mTorr, 1400 W.

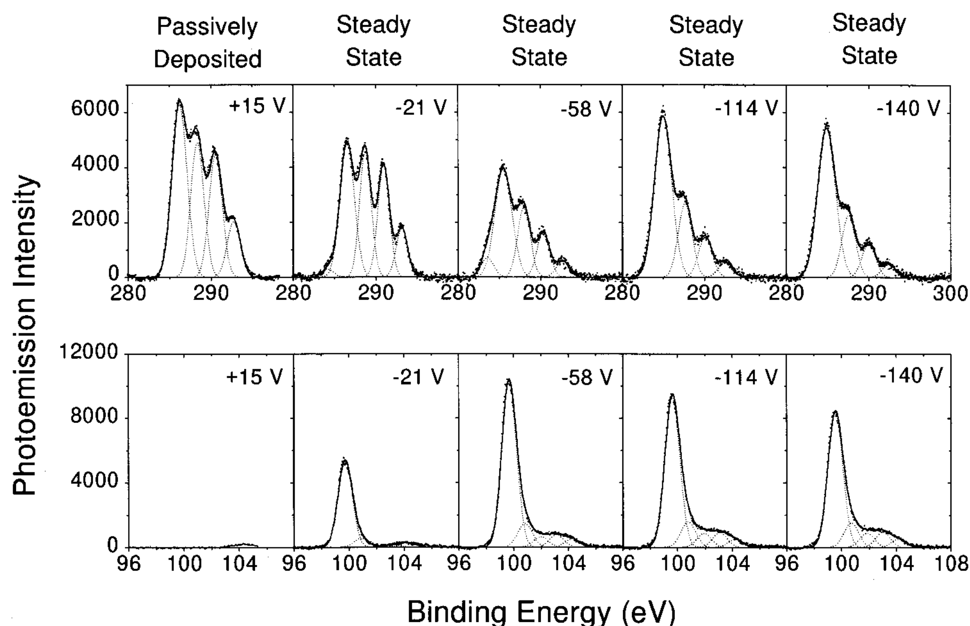

FIG. 5. XPS spectra on steady state layers and passively deposited fluorocarbon layers. The upper panels show the C(1*s*) electron emission and the lower panels the Si(2*p*) electron emission. The electrons were collected at 90°. The samples were processed in a 40 sccm CHF_3 discharge at 6 mTorr and maintained by 600 W inductive power.

was performed during the etching of crystalline silicon. Assuming that the surface can be modeled by two stacked layers on top of the bulk silicon, i.e., a fluorocarbon (CF_x) and a fluorinated silicon (SiF_y) layer, the thicknesses of these layers were obtained. For the refractive index of the CF_x layer, a value of 1.40–1.45 was taken which was determined by ellipsometry measurements on thick (>100 nm) fluorocarbon films that were passively deposited. The refractive index for the SiF_y layer and bulk silicon were set at $3.866 - i \cdot 0.8$ (Ref. 19) and $3.866 - i \cdot 0.028$,[18] respectively. The resulting layer thicknesses are plotted in Fig. 4. As opposed to etching of SiO_2, which is typically covered by a CF_x layer of less than 1.5 nm,[9,13] the etching of silicon occurs through a CF_x layer of 2–7 nm. The penetration depth of ions in the energy range investigated is about 1 nm,[24] and direct ion impact on the bulk silicon can be excluded. Neutral etch precursor transport through the CF_x layer is therefore suggested to play an important role in the etching process of the silicon. However, as can be seen from Figs. 2 and 4, both the CF_x layer thickness and the silicon etch rate depend on the ion energy. Therefore, in addition to a neutral etchant flux, an ion flux must also be considered in the interpretation of the data.

The increase in inductive power from 600 to 1400 W in a CHF_3 discharge results in an increase in both the ion current density and the passive deposition rate. In this case, the CF_x layer thickness increases and a lower silicon etch rate can be observed. Also, the addition of 12 sccm H_2 to a C_3F_6 discharge leads to a lower etch rate and a more suppressing CF_x layer. For C_2F_6 fast silicon etching is observed where the etching is regulated by a relatively thin CF_x layer. A C_2F_6 plasma is more fluorine rich than plasmas with the other feedgas chemistries. In this case the polymerization on the silicon substrate is more suppressed.

C. Surface analysis: XPS

XPS analysis was performed on polycrystalline Si samples. The samples were etched in CHF_3, C_3F_6, C_3F_6/H_2, and C_2F_6 plasmas for various bias conditions. Low resolution survey spectra showed that the surface stoichiometry mainly contained carbon, fluorine, and silicon. In addition to carbon and fluorine introduced by the feedgas, a small amount of oxygen is present on the silicon sample. This oxygen is most likely due to erosion of the quartz coupling window as is observed in other high density plasma reactors.[22,23,26,27] XPS analysis on relatively thick (>100 nm) passively deposited fluorocarbon films quantified the surface contamination as approximately 1% oxygen and 0.5% silicon. The effect of oxygen on the etching process can therefore be neglected.

To obtain information about the surface chemistry, high resolution C(1*s*) and Si(2*p*) electron emission spectra were obtained. The upper left panel of Fig. 5 shows the C(1*s*) spectrum for a 300-nm-thick fluorocarbon layer deposited on an unbiased Si sample. The samples were processed in a 6 mTorr CHF_3 plasma maintained by 600 W inductive power. The spectrum is deconvoluted in its chemical contributions ($C-CF_n$, C–F, $C-F_2$, and $C-F_3$) using a least-squares fitting technique including Gaussian peaks and a linear background. The $C-F_{1,2,3}$ bonds have a relatively well defined stoichiometric environment as opposed to the $C-CF_n$ bond. Therefore, the chemical shifts between the $C-F_1$, $C-F_2$, and the $C-F_3$ are fixed at 2.35 ± 0.15 eV with an individual width of 2.3 ± 0.2 eV full width at half-maximum (FWHM). The po-

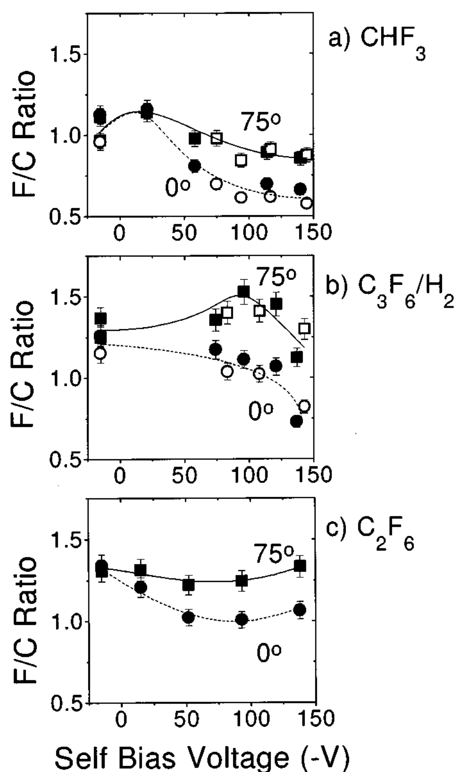

FIG. 6. F/C ratio scanned by XPS under two different emission angles, 0° and 75°. The +15 V corresponds to passively deposited fluorocarbon films. The higher voltages correspond to steady state fluorocarbon layers. (a) 40 sccm CHF_3, 6 mTorr, for two inductive powers: closed symbols 600 W, open symbols 1400 W; (b) 20 sccm C_3F_6, 6 mTorr, 1400 W, with hydrogen addition: closed symbols 0 sccm H_2, open symbols 12 sccm H_2; (c) 40 sccm C_2F_6, 6 mTorr, 1400 W.

sition of the $C–F_2$ was found to be 290.3±0.3 eV. The chemical environment of the $C–CF_n$ is not well defined and its position (285.5±0.5 eV) and FWHM (3±1 eV) were fitted. An additional peak at 283.4±0.3 eV is in some cases required to take the C–C or the C–Si bond into account. The fitted backgrounds are subtracted in Fig. 5 allowing for a direct comparison between the different C(1*s*) spectra. The other four C(1*s*) spectra were taken on crystalline silicon samples processed under biased conditions. For these conditions, a steady state CF_x layer was formed on the sample. The effect of biasing is clearly visible in the defluorination of the CF_x layer.

The change in fluorination under ion bombardment was also measured for CHF_3, C_3F_6, C_3F_6/H_2, and C_2F_6 plasmas maintained at 1400 W inductive power. Figure 6 shows the ratio of atomic density of fluorine and carbon (F/C ratio). The F/C ratio was determined for the first few fluorocarbon monolayers by collecting electrons at an emission angle of 75° with respect to the normal of the sample. The F/C ratio scanned at 0° provides stoichiometric information to a depth of about 2–3 nm. Typically, the fluorine concentration is higher at the CF_x surface. This shows that there is a gradient in the fluorine concentration towards the silicon.

For CHF_3 a similar behavior in defluorination can be observed when the inductive power is increased from 600 to 1400 W. There is no significant change in the F/C ratio, while the silicon etch rate and the CF_x layer thickness are dramatically influenced by the increase in inductive power. Also, the addition of 12 sccm H_2 to 20 sccm C_3F_6 has no significant effect on the F/C ratio, whereas the silicon etch rate is suppressed by a factor of 4. The fluorine scavenging by hydrogen seems only to affect the fluorine flux towards the silicon interface, rather than the fluorine flux that determines the F/C ratio of the steady state layer. It may, therefore, be suggested that the F/C ratio of fluorocarbon layers is mainly controlled by the ion energy and the choice of the fluorocarbon feedgas. Ellipsometry showed that the refractive index of passively deposited fluorocarbon films changed from 1.40 to 1.52 upon the addition of 12 sccm H_2. Since no significant change in the F/C ratio was observed, the change in refractive index can be ascribed to the incorporation of hydrogen in the fluorocarbon layer. Most likely, the fluorine flux towards the silicon surface is decreased by additional HF formation in the fluorocarbon layer.

Information about the fluorination of the bulk silicon during plasma exposure is obtained by high resolution scans of the Si(2*p*) electron emission. The lower left panel in Fig. 5 shows the presence of SiO_xF_y bonds in a passively deposited fluorocarbon film (300 nm). High resolution O(1*s*) scans showed that the amount of oxygen originating from the window is independent of the self-bias voltage for constant feedgas chemistry and inductive power. Therefore, it is assumed that the amount of silicon originating from the window is also independent of the self-bias power. The SiO_xF_y signal can then be interpreted as a background signal due to sputter deposition from the quartz coupling window. The four other panels show the Si(2*p*) spectra for crystalline Si under bias conditions. The Si(2*p*) spectra were deconvoluted using multiple spin-orbit split doublets (spin-orbit separation 0.60 eV and branching ratio of 0.54).[28] The doublets are separated by 1.15 eV,[29] which represents the chemical shifts of SiF_y ($y=1$, 2, 3, 4). The elemental Si peak was found to be at 99.5±0.1 eV. It can be concluded that an increase in the self-bias voltage leads to a more fluorinated silicon surface as previously observed.[30]

Figure 5 shows a minimum in the C(1*s*) intensity as function of the self-bias voltage, suggesting a minimum in the CF_x layer thickness. The maximum in the elemental Si intensity indicates that also the total layer (CF_x+SiF_y) thickness has a minimum as a function of the self-bias voltage. A similar behavior is observed by the ellipsometry surface analysis in Fig. 4. A more careful analysis of the XPS spectra shows that both ellipsometry and XPS lead to consistent results; see Fig. 7. For this analysis, the CF_x layer thickness (d_{CF_x}) is calculated from the integrated C(1*s*) photoemission intensities ($I^{\text{stst}}_{C(1s)}$) in Fig. 5 using the integrated intensity ($I^{\text{dep}}_{C(1s)}$) of the passively deposited layer as a reference intensity:[31]

$$d_{CF_x}=\lambda_{C(1s)}\ \ln\left(1-\frac{I^{\text{stst}}_{C(1s)}}{I^{\text{dep}}_{C(1s)}}\right)^{-1}. \tag{1}$$

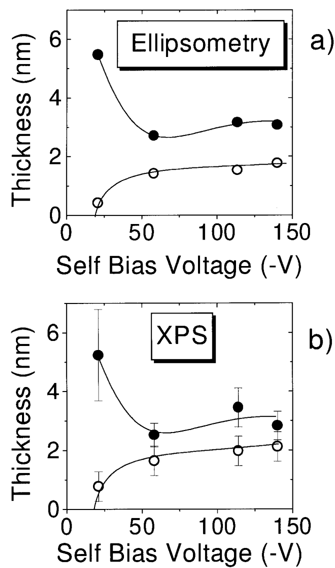

FIG. 7. CF_x and SiF_y layer thicknesses determined by (a) ellipsometry and (b) XPS. The samples analyzed were processed in a 40 sccm CHF_3 discharge at 6 mTorr and maintained by 600 W inductive power.

Here $\lambda_{C(1s)}$ is the mean free path of the C(1*s*) photoelectrons in the CF_x layer. The superscripts stst and dep refer to the steady state and passively deposited CF_x layers, respectively. The CF_x layer thicknesses determined by XPS reproduced the ellipsometry results when a value of 3.5 ± 0.5 nm was used for $\lambda_{C(1s)}$. The SiF_y layer thickness (d_{SiF_y}) was determined using the intensities of the elemental and the chemically shifted Si(2*p*) emissions, $I^{Si}_{Si(2p)}$ and $I^{SiF_y}_{Si(2p)}$ respectively:[31]

$$d_{SiF_y}=\lambda_{Si(2p)}\ \ln\left(1+\frac{I^{SiF_y}_{Si(2p)}}{KI^{Si}_{Si(2p)}}\right). \tag{2}$$

Here $\lambda_{Si(2p)}$ is the mean free path of the C(1*s*) photoelectrons in the SiF_y layer. *K* is the ratio of the atomic density of Si atoms in the SiF_y layer and the bulk silicon. *K* can be calculated using the intensities of the chemical shifted peaks in the Si(2*p*) spectrum. The spectra shown in Fig. 5 correspond to a value of $K=0.31\pm0.02$. Similar to thermal SiO_2, $\lambda_{Si(2p)}$ was set to 2.5 nm.[31] Figure 7 shows that XPS analysis confirms the results on the CF_x and SiF_y layers obtained by ellipsometry.

IV. MODELING OF THE DATA

The surface analysis results showed that the etching of silicon is regulated by a relatively thick fluorocarbon layer. In this case there is no direct ion impact on the bulk silicon possible and most likely there is a neutral transport of reactive fluorine through the fluorocarbon layer required to etch silicon. Oehrlein *et al.*[10,11] proposed a transport mechanism including a diffusion process for low ion density etching of silicon, based on the observation of an inversely proportional relationship between the silicon etch rate and the CF_x layer thickness. However, in a high density discharge the ion to

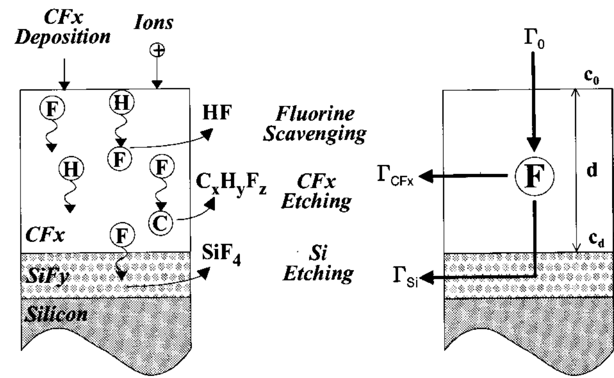

FIG. 8. Schematic of the model presented. The left-hand portion shows the processes in the CF_x layer. The portion on the right-hand side indicates three fluorine fluxes. Γ_0 is the fluorine flux in the CF_x layer. Γ_{CF_x} is the fluorine flux that is used to form desorbing fluorocarbon species. This flux is required to balance the fluorocarbon deposition that occurs during the etching process. Γ_{Si} is the fluorine flux that reacts with the silicon to form volatile SiF_4 in the SiF_y layer.

neutral ratio is at least a factor of 100 higher. (The ion densities are typically 10^{12} cm^{-3} for an ICP and 10^{10} cm^{-3} for a RIE system at a similar pressure.) Figures 2 and 4 also show that as function of the self-bias voltage the CF_x layer thickness is not necessarily decreasing while the etch rate is increasing. In Secs. IV A–IV D a model will be derived that includes the effect of ion bombardment on steady state etching.

A. Proposed mechanism

Fluorocarbon material shows no significant etch rate in an atomic fluorine environment.[32] The etch rate of fluorocarbon material by physical sputtering in an argon plasma is also significantly lower than the fluorocarbon etch rate in fluorocarbon plasmas at similar ion current densities and ion energies.[14] It is the combination of the fluorine species and the ion bombardment that results in significant fluorocarbon etching. Silicon spontaneously etches in an atomic fluorine environment.[33] Our model assumes that atomic fluorine is the precursor of silicon etching. In addition, fluorine is also consumed by the ion induced etching of the CF_x layer. This leads to the formation of desorbing fluorocarbon species. A schematic picture of the model is presented in Fig. 8.

Atomic fluorine is produced in the discharge by dissociation processes and possibly by ion impact fragmentation and film dissociation at the substrate surface. Atomic fluorine can diffuse through the CF_x layer and react with the CF_x layer and thus contribute to etching of the CF_x layer. This process is enhanced by the energy transferred from ion impact. Fluorocarbon deposition is being suppressed when the flux of desorbing fluorocarbon species is higher than the carbon flux of the adsorbing fluorocarbon species from the gas phase. In steady state, the adsorbing and desorbing carbon fluxes are balanced. Steady state also requires that the fluorine to carbon ratio of the desorbing flux is at least lower than the fluorine to carbon ratio of the adsorbing flux (including the atomic fluorine flux from the gas phase). Additionally, the

ion impact must provide enough energy to enhance the production of the desorbing flux. Figures 2 and 4 show that etching only occurs when the ion energy exceeds a certain threshold energy. This threshold energy depends on various plasma process parameters, for example, feedgas chemistry or inductive power. For the modeling, it is assumed that desorbing fluorocarbon species are only produced *in* the fluorocarbon layer. At this point, any effect of sputtering at the fluorocarbon surface is neglected, but will be included in Sec. IV D. In steady state, fluorine also reacts with silicon, resulting in the formation of volatile SiF_4. Figure 8 also depicts the influence of hydrogen. This will be discussed later. Since angle resolved XPS in Fig. 6 indicated that the fluorine concentration is decreasing in the fluorocarbon layer towards the bulk silicon, it is assumed that silicon etching is limited by the fluorine supply rather than by the transport of SiF_4 or volatile fluorocarbon species to the gas phase.

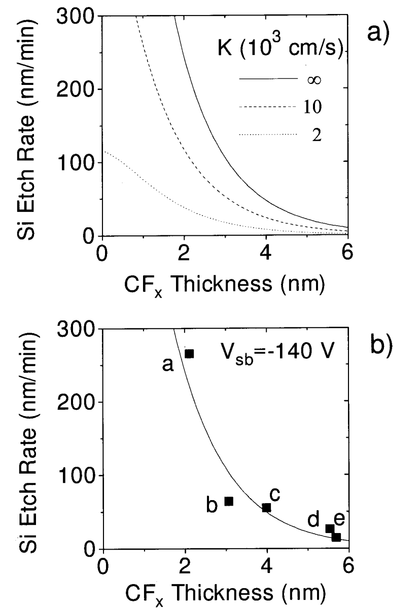

FIG. 9. Silicon etch rate vs CF_x layer thickness. (a) The model. (b) The experimental data in comparison with an exponential fit ($y=A\ \exp(-Bx)$). In (b) a: C_2F_6 1400 W; b: CHF_3 600 W; c: C_3F_6 1400 W; d: CHF_3 1400 W; e: C_3F_6/H_2 1400 W.

B. Mathematical description

Our model assumes that the fluorine flux through the CF_x layer is partially consumed by the CF_x layer and the SiF_y layer. As shown in Fig. 8, the atomic fluorine flux that enters the CF_x layer, Γ_0, is equal to the sum of the fluorine fluxes Γ_{CF_x} and Γ_{Si}:

$$\Gamma_0=\Gamma_{CF_x}+\Gamma_{Si}. \tag{3}$$

Γ_{CF_x} and Γ_{Si} represent the fluorine fluxes that are used for the formation of desorbing fluorocarbon species (including HF) and SiF_4, respectively. The consumption of fluorine in a small length dx in the CF_x layer is proportional to the fluorine concentration c and a reaction rate constant κ. The change $d\Gamma$ in the fluorine flux Γ is therefore

$$d\Gamma=-\kappa c dx. \tag{4}$$

Applying Fick's law, $\Gamma=-Ddc/dx$, and introducing a diffusion constant D, Eq. (4) can be rewritten as

$$D\frac{d^2c}{dx^2}-\kappa c=0. \tag{5}$$

In general the rate constant κ and the diffusivity D may depend on the depth in the CF_x layer, since neither the energy deposition of the ion bombardment nor the material density is necessarily uniform across the CF_x layer. For simplicity, however, it is assumed that both κ and D are independent of the depth x. This assumption allows for an analytical approach which still qualitatively agrees with the presented data. The general solution of Eq. (5) is given by

$$c(x)=c_1\ \exp(-\sqrt{\kappa/D}x)+c_2\ \exp(\sqrt{\kappa/D}x). \tag{6}$$

$\sqrt{D/\kappa}$ is the attenuation length of the atomic fluorine in the CF_x layer and will be determined later on in this section. The concentrations c_1 and c_2 are constants and can be determined using the following boundary conditions:

$$c(0)=c_0,\qquad -D\frac{dc}{dx}\bigg|_{x=d}=\Gamma_{Si}=Kc_d. \tag{7}$$

Here c_0 is the atomic fluorine concentration at the top of the CF_x layer. The second boundary condition is Fick's law applied to the silicon interface at $x=d$. The boundary condition of steady state silicon etching is also applied to the latter. Silicon spontaneously etches with the atomic fluorine at the silicon surface. The incoming fluorine flux Γ_{Si} at the silicon interface must leave as SiF_4 in a steady state situation. The silicon etch rate is assumed to be proportional to the fluorine concentration c_d by a reaction constant K. With this set of equations [Eqs. (6), (7), and Fick's law] it is possible to obtain a relationship between the silicon etch rate, expressed in terms of Γ_{Si}, and the CF_x layer thickness d:

$$\Gamma_{Si}=\frac{c_0\sqrt{\kappa D}}{\left[\sqrt{\kappa D}K^{-1}+\tanh\left(\sqrt{\frac{\kappa}{D}}d\right)\right]\cosh\left(\sqrt{\frac{\kappa}{D}}d\right)}. \tag{8}$$

The silicon etch rate is inversely proportional to the CF_x layer thickness d as shown in Fig. 9. The values of c_0, κ, and D are fixed at $5\times10^{15}\ cm^{-3}$, $10^8\ s^{-1}$, and $10^{-6}\ cm^2/s$ and are determined later on. The effect of the substrate is included in the reaction rate constant K. Decreasing this reactivity, keeping c_0, κ, and D fixed, results in a different relationship between the etch rate and the CF_x layer thickness. Equation (8) may therefore explain that different CF_x layer thicknesses are observed on different substrates by including the etch rate behavior of the substrate in Eq. (7) as a function of the fluorine concentration at the substrate interface.

In order to get an estimate for the attenuation length $\sqrt{D/\kappa}$ of the atomic fluorine concentration in the CF_x layer, the silicon etch rate at a constant self-bias voltage of -140 V is plotted versus the CF_x layer thickness for the various feedgas chemistries in the second panel in Fig. 9. The data points were fitted using an exponential decay, which approximates Eq. (8) for thick fluorocarbon layers and $K=\infty$. The fit resulted in a value of about 1 nm for $\sqrt{D/\kappa}$ and 5×10^{16} $cm^{-2}\,s^{-1}$ for $c_0\sqrt{\kappa D}$. It should be noted that this is a very rough estimate. This estimate assumes that the fluorine concentration c_0 and the transport parameters κ and D are constant for the various feedgas chemistries. The fluorine flux required to suppress the polymerization, Γ_{CF_x}, is in this case the varying parameter between the various feedgas chemistries and determines the CF_x layer thickness and the silicon etch rate. It may be expected, however, that in addition to Γ_{CF_x} c_0, κ, and D also depend on the plasma conditions and, therefore, on the feedgas chemistry and inductive power level. Since our data do not provide enough information about the plasma state, we limit ourselves mainly to the effect of biasing. The plasma generation is in our case independent of the bias power. We continue the modeling in order to see how biasing can affect parameters like Γ_{CF_x}, c_0, κ, and D, rather than pointing out the effect of the plasma conditions on these parameters. The estimate of $\sqrt{D/\kappa}$ and $c_0\sqrt{\kappa D}$ will be used to estimate the order of magnitude of the parameters κ, D, c_0, and Γ_{CF_x}.

A second result that can be derived using Eqs. (6), (7), and Fick's law is an expression for the fluorine flux Γ_0 into the CF_x layer:

$$\Gamma_0=\frac{c_0\sqrt{\kappa D}\sinh\left(\sqrt{\frac{\kappa}{D}}\,d\right)+\Gamma_{Si}}{\cosh\left(\sqrt{\frac{\kappa}{D}}\,d\right)}. \tag{9}$$

For rather thick CF_x layers, i.e., $d\gtrsim3\sqrt{D/\kappa}$, the silicon has no significant effect on the fluorine flux Γ_0 into the CF_x layer. The fluorine flux Γ_0 into the CF_x layer is therefore independent of the layer thickness d, which can easily be shown using Eqs. (8) and (9):

$$\Gamma_0\approx c_0\sqrt{\kappa D}. \tag{10}$$

In order to solve Eqs. (8) and (9) for d and Γ_{Si} the constraint for steady state etching has to be satisfied, i.e., in order to have a steady state situation a fluorine flux Γ_{CF_x} must leave the surface as etched fluorocarbon species. The total reacted fluorine in the CF_x layer is equal to the integral of Eq. (4):

$$\Gamma_{CF_x}=\int_0^d \kappa c\,dx, \tag{11}$$

which is equivalent to Eq. (3). The CF_x layer thickness d is adjusted in such a way that the fluorine used for the etching of fluorocarbon material in the CF_x layer cancels the fluorocarbon deposition. For solving Eqs. (3), (8), and (9) a numerical approach is required. To gain better insight on the influence of parameters like κ, D, c_0, and Γ_{CF_x}, here we only include an analytical solution for a relatively thick CF_x layer, i.e., $d\gtrsim3\sqrt{D/\kappa}$. As a result of this assumption, the fluorine consumption by the silicon etching is also independent of the layer thickness [using Eqs. (3) and (10)]:

$$\Gamma_{Si}\approx c_0\sqrt{\kappa D}-\Gamma_{CF_x}. \tag{12}$$

Equating the layer thickness yields the following expression [using Eq. (8)]:

$$d\approx-\sqrt{\frac{D}{\kappa}}\ln\left[\frac{1}{2}\left(1-\frac{\Gamma_{CF_x}}{c_0\sqrt{\kappa D}}\right)\left(1+\frac{\sqrt{\kappa D}}{K}\right)\right]. \tag{13}$$

Equations (12) and (13) clearly show that etching is only possible when $\Gamma_{CF_x}/c_0\sqrt{\kappa D}<1$. At the threshold voltage, where etching of the substrate starts to occur, the ratio is equal to 1. From Fig. 2 it is clear that this ratio must depend on the self-bias voltage. Two possible roles of ion bombardment on the etching process will be investigated in Secs. IV C–IV D.

C. Ion enhanced transport of fluorine from the gas phase to the silicon interface

The main source of atomic fluorine may originate from the gas phase and be transported through the CF_x layer by an ion enhanced mechanism. In this case, both the concentration c_0 of atomic fluorine at the gas phase interface and the fluorine consumption Γ_{CF_x} in the CF_x layer are assumed to be independent of the self-bias voltage, Γ_{CF_x} and c_0 are determined by the plasma state, i.e., c_0 and Γ_{CF_x} are functions of the feedgas chemistry, flow, pressure, and inductive power. In order to make a transition from a deposition mode $(\Gamma_{CF_x}/c_0\sqrt{\kappa D}>1)$ to an etching mode $(\Gamma_{CF_x}/c_0\sqrt{\kappa D}<1)$ for a given plasma state, the factor $\sqrt{\kappa D}$ has to increase as a function of the self-bias voltage.

It is likely that the diffusivity of the fluorine atoms increases at higher self-bias voltages, since the wafer temperature is expected to increase from 10 to 30 °C depending on the bias power. Experiments, carried out by Pasternak *et al.*[34,35] for several gases, except atomic fluorine, show that this increase in temperature can lead to an increase in the diffusivity by a factor of 5 in polymers. The diffusivity may be even further enhanced by ion induced porosity of the CF_x layer. Based on Pasternak's data, we estimate the diffusivity of atomic fluorine to be of the order of 10^{-6} cm^2/s.

Beside ion enhanced diffusion, the reactivity of fluorine with the CF_x layer is also likely to increase, since, as mentioned before, ion bombardment is required for the etching of the CF_x layer. The energy that is provided by the ions may initiate chemical reactions of fluorine in the CF_x layer upon which volatile fluorocarbon species are formed. Section IV B showed that the length $\sqrt{D/\kappa}$ is of the order of 1 nm under etching conditions. This corresponds to a value of about 10^8 s^{-1} for the reactivity κ.

A reasonable suggestion for the dependence of $\sqrt{\kappa D}$ on the self-bias voltage is shown in the first panel of Fig. 10.

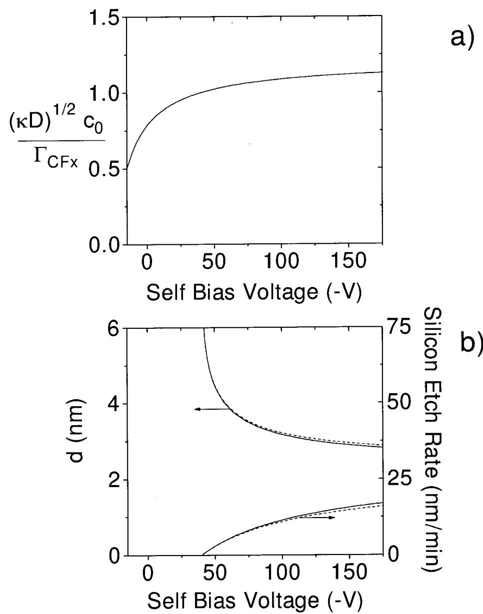

FIG. 10. CF_x layer thickness (d) and the silicon etch rate (Γ_{Si}) as a function of the self-bias voltage according to the model presented. In (a) the input that is used, which can be explained by an enhancement in the diffusion transport or by ion impact fragmentation and surface dissociation is shown. The solid lines in (b) represent the numerical solutions of Eqs. (3), (8), and (9). The dashed lines represent the analytical solutions given by Eqs. (12) and (13).

$\sqrt{\kappa D}$ is scaled with Γ_{CF_x} and c_0 which are kept constant at 4.5×10^{16} cm^{-2} s^{-1} and 5×10^{15} cm^{-3}, respectively. When no bias is applied, the ions are still accelerated towards the wafer by the floating potential. The factor $\sqrt{\kappa D}$ has, therefore, a finite value, but is not high enough to suppress the deposition of fluorocarbon material. A numerical solution of Eqs. (3), (8), and (9) is plotted in the second panel. For simplicity, it is assumed that $\sqrt{D/\kappa}$ is independent of the self-bias voltage and $K \gg \sqrt{\kappa D}$. A comparison with the data in Figs. 2 and 4 shows a good qualitative resemblance with our model if the factor $\sqrt{\kappa D}$ levels out at higher self-bias voltages. A minimum in the CF_x layer thickness could be obtained by assigning a dependency on the self-bias voltage for the diffusivity D and the rate constant κ such that both $\sqrt{D/\kappa}$ and $\sqrt{\kappa D}$ are increasing as a function of the self-bias voltage. It can be concluded that our model is consistent with the experimental data if an ion enhanced transport of fluorine is included.

D. Ion impact fragmentation and film dissociation

Equations (12) and (13) show that the ratio $\Gamma_{CF_x}/c_0\sqrt{\kappa D}$ must be smaller than 1 in order to have steady state etching of silicon. Beside ion enhanced transport of fluorine through the CF_x layer (previous case), it is also possible that the ratio $\Gamma_{CF_x}/c_0\sqrt{\kappa D}$ is decreasing as a function of the self-bias voltage due to ion impact fragmentation and dissociation of the CF_x surface molecules.[36,37] In order for these surface processes to be a source of fluorine, the carbon must be more likely to desorb from the CF_x surface than the fluorine at higher self-bias voltages, i.e., the desorbing stoichiometry depends on the self-bias voltage. In this case we keep the transport parameters κ and D constant and we assume that c_0 and Γ_{CF_x} are functions of the self-bias voltage. Γ_{CF_x} will decrease as a function of the self-bias voltage if the fluorocarbon deposition is partially suppressed by ion sputtering of the CF_x layer at the surface. This sputtering may be enhanced by the presence of fluorine. The concentration c_0 of atomic fluorine at the gas phase interface may increase as a function of the self-bias voltage due to more complete ion fragmentation and film dissociation. The fluorine concentration c_0 saturates at higher voltages, since ions and surface molecules have a finite number of fluorine atoms. The first panel of Fig. 10 shows again the suggested dependence of the ratio $c_0\sqrt{\kappa D}/\Gamma_{CF_x}$ on the self-bias voltage. It is assumed that the ratio saturates around 50 eV ion energy. The second panel shows a numerical solution keeping the other parameters constant ($\kappa=10^8$ s^{-1} and $D=10^{-6}$ cm^2/s) and $K \gg \sqrt{\kappa D}$. This assumption shows good agreement with the data presented in Figs. 2 and 4, but cannot explain a minimum in the CF_x layer thickness. As shown in previous Sec. IV C a second assumption about the diffusivity D and absorption rate constant κ as a function of the self-bias voltage may explain a minimum in the CF_x layer thickness.

E. Effect of hydrogen addition on the etching process

Hydrogen is well known for its deep penetration into the substrate (10–30 nm)[24] and for fluorine scavenging in the reactor and in the CF_x layer.[4,10,38,39] The effect of hydrogen addition in a fluorocarbon plasma can easily be included in our model. First of all, hydrogen will reduce the fluorine concentration c_0 due to the formation of volatile HF in the gas phase and at the CF_x surface. Second, the atomic fluorine consumption Γ_{CF_x} in the CF_x layer will increase as hydrogen penetrates the CF_x layer, since volatile HF is formed in addition to desorbing fluorocarbon species. Also the reaction rate constant κ may increase upon hydrogen addition. The first panel in Fig. 11 shows the suggested ratio $\Gamma_{CF_x}/c_0\sqrt{\kappa D}$ with and without hydrogen addition. It is assumed that the transport parameters κ and D are not affected by the hydrogen addition. The second panel shows the corresponding CF_x layer thicknesses and Si etch rates according to a numerical solution of the model presented and is qualitatively consistent with the data in Figs. 2 and 4. (The parameters Γ_{CF_x}, c_0, κ, and D in Fig. 11 are of the same order as those presented earlier.)

F. Relation between fluorocarbon etching and silicon etching

Figures 2 and 3 show that the fluorocarbon and the silicon etch rate have the same dependency on various process parameters, e.g., the self-bias voltage. For the etching of a thick (>50 nm) fluorocarbon layer, the fluorine flux Γ_0 into the CF_x is independent of the thickness and is given by Eq. (10). In order to balance the fluorocarbon deposition, a fluorine

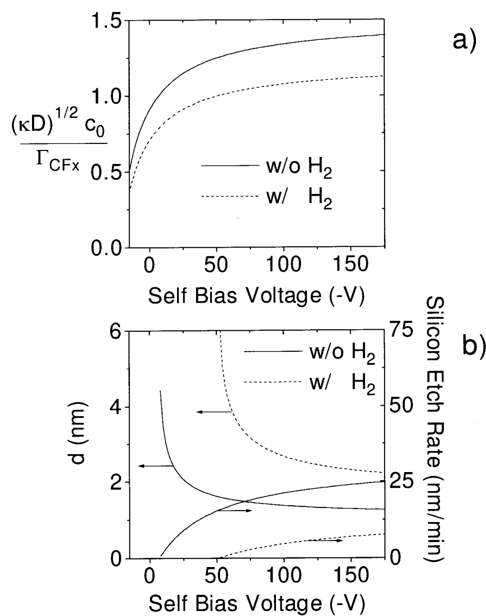

FIG. 11. Effect of hydrogen addition (a) on the ratio $c_0\sqrt{\kappa D}/\Gamma_{CF_x}$ and (b) on the CF_x layer thickness and Si etch rate.

flux Γ_{CF_x} is required for the formation of desorbing fluorocarbon species. When this flux is smaller than the entering fluorine flux ($\Gamma_{CF_x}<\Gamma_0$), the resulting fluorine flux (Γ_0-Γ_{CF_x}) is used for the net etching of the thick fluorocarbon layer. From Eqs. (3) and (10) it can be concluded that this fluorine flux is equal to the flux that would react with a silicon substrate during steady state etching [Eq. (12)]. The silicon etch rate and the fluorocarbon etch rate differ, therefore, only by a constant factor for various process conditions. This factor compensates for the difference in chemical composition between a silicon substrate and a thick fluorocarbon layer. First of all, the amount of fluorine required to form volatile species depends on the substrate. For example, to etch silicon, four fluorine atoms per silicon atom are required to form SiF_4, whereas the average amount of fluorine required to remove a carbon atom from a fluorocarbon substrate may be different. Second, the density of the substrate has to be included in order to convert the etching fluorine flux to an etch rate.

Beside silicon, for nitride[40] and photoresist[41] too, the etch rate was found to be linear in the fluorocarbon etch rate for similar process conditions in the same experimental setup. Assuming that the etching of both nitride and photoresist is fluorine driven, it can be explained by the model that the etching of these materials is also similar to fluorocarbon etching.

V. CONCLUSIONS

The etching of silicon is studied in a high density inductively coupled plasma reactor utilizing various fluorocarbon feedgases (CHF_3, C_3F_6, C_3F_6/H_2, and C_2F_6). Ellipsometry and x-ray photoelectron spectroscopy consistently showed that during steady state etching the silicon surface is covered by a relatively thick fluorocarbon layer varying from 2 to 7 nm. The ion energy was varied up to 150 eV. The rate of direct ion impact on the silicon substrate at this energy is probably low compared to the silicon etch rate. Therefore, a mechanism based on a neutral fluorine transport through the fluorocarbon layer is suggested. Silicon can be etched by forming volatile SiF_4, which can diffuse through the fluorocarbon layer into the gas phase. Since XPS showed that the fluorine concentration in the fluorocarbon layer decreases towards the silicon interface, it is likely that the etching is limited by a fluorine diffusion transport through the fluorocarbon layer. The fluorine transport through the fluorocarbon layer is described by a diffusion mechanism based on Fick's law. A condition for steady state etching of silicon can be derived, assuming that, in addition to silicon, the fluorocarbon layer also reacts with the fluorine. This leads to the formation of desorbing fluorocarbon species, which balances the fluorocarbon deposition during the etching process.

Despite the fact that direct ion impact on the silicon substrate is probably negligible, it is found that the ion energy is an important parameter in the etching of silicon. Our model includes two possible roles of the ions. The first role may be the enhancement in the diffusivity of fluorine atoms in the fluorocarbon layer and the enhancement in the reaction probability of fluorine in the fluorocarbon layer. In this case the fluorine is originating from the gas phase. The second role may be ion impact fragmentation and dissociation of the surface fluorocarbon molecules. Both roles suggested lead to a similar description of the etch rate and the fluorocarbon layer thickness that is consistent with the experimental data.

The role of hydrogen on the etching process was also investigated. From a change in the refractive index of thick passively deposited fluorocarbon layers, it can be concluded that the composition of the fluorocarbon layer changes upon hydrogen addition. However, XPS showed that the F/C ratio of the fluorocarbon layer is not significantly affected when hydrogen is added to the discharge. The F/C ratio is primarily determined by the ion energy and the choice of the fluorocarbon feedgas. It can therefore be concluded that the hydrogen is incorporated into the fluorocarbon layer. The hydrogen in the fluorocarbon layer suppresses the fluorine flux towards the silicon interface by the formation of volatile HF in a steady state fluorocarbon layer. This results in a thicker fluorocarbon layer and the suppression of the silicon etch rate. The influence of hydrogen addition on the silicon etch rate and the fluorocarbon layer thickness can be included in our model and was found to be consistent with the experimental data.

ACKNOWLEDGMENTS

The authors would like to thank M. C. M. van de Sanden, G. J. H. Brussaard, and R. J. Severens from Eindhoven University of Technology for their helpful discussions. They are also grateful to M. F. Doemling, J. M. Mirza, B. E. E. Kastenmeier, and P. J. Matsuo for their supporting work and ideas. This work was financially supported in part by Lam

Research and the New York State Science and Technology Foundation. The authors also would like to thank the Netherlands Organization for International Cooperation in Higher Education (NUFFIC) for providing the Stimuleringsprogramma voor Internationalisering van Wetenschappelÿk Ouderwÿs (STIR WO) grant and Eindhoven University of Technology for their Mignot grant that allowed the exchange of students between Eindhoven University of Technology and the State University of New York at Albany.

[1]J. H. Keller, J. C. Forster, and M. S. Barnes, J. Vac. Sci. Technol. A **11**, 2487 (1993).
[2]N. R. Rueger, M. Schaepkens, M. F. Doemling, J. J. Beulens, J. M. Mirza, T. E. F. M. Standaert, R. M. A. Driessens, and G. S. Oehrlein (unpublished).
[3]R. A. H. Heinecke, Solid-State Electron. **18**, 1146 (1975).
[4]L. M. Ephrath, J. Electrochem. Soc. **126**, 1419 (1979).
[5]G. S. Oehrlein, P. J. Matsuo, M. F. Doemling, N. R. Rueger, B. E. E. Kastenmeier, M. Schaepkens, T. E. F. M. Standaert, and J. J. Beulens, Plasma Sources Sci. Technol. **5**, 193 (1996).
[6]F. H. Bell, O. Joubert, G. S. Oehrlein, Y. Zhang, and D. Vender, J. Vac. Sci. Technol. A **12**, 3095 (1994).
[7]G. S. Oehrlein, D. Zhang, D. Vender, and O. Joubert, J. Vac. Sci. Technol. A **12**, 333 (1994).
[8]J. P. Simko and G. S. Oehrlein, J. Electrochem. Soc. **138**, 2748 (1991).
[9]N. R. Rueger, J. J. Beulens, M. Schaepkens, M. F. Doemling, J. M. Mirza, T. E. F. M. Standaert, and G. S. Oehrlein, J. Vac. Sci. Technol. A **15**, 1881 (1997).
[10]G. S. Oehrlein and H. L. Williams, J. Appl. Phys. **62**, 662 (1987).
[11]G. S. Oehrlein, S. W. Robey, and M. A. Jaso, Mater. Res. Soc. Symp. Proc. **98**, 229 (1987).
[12]M. A. Lieberman and A. J. Lichtenberg, *Principles of Plasma Discharges and Materials Processing* (Wiley, New York, 1994).
[13]M. Schaepkens, Material Processing in a Transformer Coupled Plasma Source, Eindhoven University of Technology, Master's Thesis (1996).
[14]T. E. F. M. Standaert, Deposition and Etching in Inductively Coupled Fluorocarbon Plasmas, Eindhoven University of Technology, Master's Thesis (1996).
[15]J. M. Cook, O. Turmel, T. Wicker, J. Winniczek, Lam Research Internal Report, (1994).
[16]R. M. A. Azzam and N. M. Bashara, *Ellipsometry and Polarized Light* (North-Holland, Amsterdam, 1977).
[17]J. L. Buckner, D. J. Vitkavage, E. A. Irene, and T. M. Mayer, J. Electrochem. Soc. **133**, 1729 (1986).
[18]M. Haverlag, D. Vender, and G. S. Oehrlein, Appl. Phys. Lett. **61**, 2876 (1992).
[19]G. S. Oehrlein, J. Vac. Sci. Technol. A **11**, 34 (1993).
[20]J. A. O'Neill and J. Singh, J. Appl. Phys. **77**, 497 (1997).
[21]M. Schaepkens, R. C. M. Bosch, T. E. F. M. Standaert, J. M. Cook, and G. S. Oehrlein, J. Vac. Sci. Technol. A (submitted).
[22]G. S. Oehrlein, D. Zhang, D. Vender, and M. Haverlag, J. Vac. Sci. Technol. A **12**, 323 (1994).
[23]N. R. Rueger, J. J. Beulens, M. Schaepkens, M. F. Doemling, J. M. Mirza, T. E. F. M. Standaert, S. P. L. Nijsten, and G. S. Oehrlein (unpublished).
[24]G. S. Oehrlein, R. M. Tromp, J. C. Tsang, Y. H. Lee, and E. J. Petrillo, J. Electrochem. Soc. **132**, 1441 (1985).
[25]G. S. Oehrlein, Mater. Sci. Eng. B **4**, 441 (1989).
[26]Y. Hikosaka, M. Nakamura, and H. Sugai, Jpn. J. Appl. Phys., Part 1 **33**, 2157 (1994).
[27]J. M. Mirza, R. M. A. Driessens, N. R. Rueger, M. F. Doemling, and G. S. Oehrlein (unpublished).
[28]F. R. McFeeley, J. F. Morar, N. D. Shinn, G. Landgren, and F. J. Himpsel, Phys. Rev. B **30**, 764 (1984).
[29]K. J. Gruntz, L. Ley, and R. L. Johnson, Phys. Rev. B **24**, 2069 (1981).
[30]D. Vender, M. Haverlag, and G. S. Oehrlein, Appl. Phys. Lett. **61**, 3136 (1992).
[31]D. Briggs and M. P. Seah, *Practical Surface Analysis* (Wiley, New York, 1990), Vol. 1.
[32]B. E. E. Kastenmeier, P. J. Matsuo, J. J. Beulens, and G. S. Oehrlein, J. Vac. Sci. Technol. A **14**, 2802 (1996).
[33]C. J. Mogab, A. C. Adams, and D. L. Flamm, J. Appl. Phys. **49**, 3796 (1978).
[34]R. A. Pasternak, M. V. Christensen, and J. Heller, Macromolecules **3**, 366 (1970).
[35]R. A. Pasternak, G. L. Burns, and J. Heller, Macromolecules **4**, 479 (1971).
[36]L. M. Ephrath, J. Electrochem. Soc. **126**, 1419 (1979).
[37]L. M. Ephrath and E. J. Petrillo, J. Electrochem. Soc. **129**, 2282 (1982).
[38]W. H. Chang, I. Bello, and W. M. Lau, J. Vac. Sci. Technol. A **11**, 1221 (1993).
[39]I. Bello, W. H. Chang, and W. M. Lau, J. Vac. Sci. Technol. A **12**, 1425 (1994).
[40]M. Schaepkens, T. E. F. M. Standaert, P. G. M. Sebel, J. M. Cook, and G. S. Oehrlein (unpublished).
[41]M. F. Doemling, N. R. Rueger, G. S. Oehrlein, and J. M. Cook (unpublished).